The Astrophysical Journal, 619:L167–L170, 2005 February 1

EMPIRICAL CONSTRAINTS ON THE GENERAL RELATIVISTIC ELECTRIC FIELD ASSOCIATED WITH PSR J0437−4715

C. Venter and O. C. De Jager
Unit for Space Physics, North-West University, Potchefstroom Campus, Private Bag X6001,
Potchefstroom 2520, South Africa; fskcv@puk.ac.za, fskocdj@puk.ac.za
Received 2004 June 2; accepted 2004 December 13; published 2005 January 10

ABSTRACT

We simulate the magnetosphere of the nearby millisecond pulsar PSR J0437−4715, which is expected to have an unscreened electric potential due to the lack of magnetic pair production. We incorporate general relativistic (GR) effects and study curvature radiation (CR) by primary electrons but neglect inverse Compton scattering of thermal X-ray photons by these electrons. We find that the CR spectrum cuts off at energies below ∼17 GeV, well below the threshold of the High Energy Stereoscopic System (H.E.S.S.) telescope ($\lesssim$100 GeV), while other models predict a much higher cutoff of $\gtrsim$100 GeV. GR theory also predicts a relatively narrow pulse ($\beta^o \sim$ 0.2 phase width) centered on the magnetic axis. EGRET observations above 100 MeV significantly constrain the application of the Muslimov & Harding model for γ-ray production as a result of GR frame dragging and ultimately its polar cap (PC) current and accelerating potential. Whereas the standard prediction of this pulsar's γ-ray luminosity due to GR frame dragging is ∼10% of the spin-down power, a nondetection by forthcoming H.E.S.S. observations will constrain it to $\lesssim$0.3%, enforcing an even more severe revision of the accelerating electric field and PC current.

Subject headings: pulsars: individual (PSR J0437−4715) — stars: neutron

1. INTRODUCTION

Several authors have included general relativistic (GR) frame dragging in models of pulsar magnetospheric structure and associated radiation and transport processes, recognizing it to be a first-order effect (see, e.g., Muslimov & Harding 1997, hereafter MH97; Dyks et al. 2001).

Usov (1983) was the first to suggest that the low magnetic field strengths of millisecond pulsars (MSPs) allow γ-rays up to at least 100 GeV to escape pair production. Most MSPs have (largely) unscreened electric fields due to the low optical depths of primary curvature γ-rays for pair production in such low-B pulsar magnetospheres (Harding et al. 2002, hereafter HMZ02). Radiation reaction limited curvature γ-rays up to about 100 GeV from MSPs have been predicted (HMZ02; Bulik et al. 2000, hereafter BRD00), making nearby MSPs such as PSR J0437−4715 (Johnston et al. 1993) attractive targets for ground-based γ-ray groups (BRD00; C. Venter 2004, unpublished). The unscreened case offers a test for fundamental GR electrodynamic derivations of the polar cap (PC) current and potential, without having to invoke additional modifications such as pair formation fronts (Harding & Muslimov 1998, hereafter HM98) with associated slot gaps (Muslimov & Harding 2003) to explain most observations of canonical (high-B) pulsars.

The use of an unscreened GR electric field (see § 2) for PSR J0437−4715 (implied by its relatively low spin-down power; HMZ02) was justified a posteriori (see § 3). Several important parameters, most notably its mass and distance (Van Straten et al. 2001), are accurately known, making PSR J0437−4715 one of the closest pulsars to Earth and probably much brighter and more easily observed than other MSPs. Also, observations show that the radio and X-ray beams virtually coincide (Zavlin et al. 2002), implying that the observer sweeps through the approximate center of the PC (Manchester & Johnston 1995; Gil & Krawczyk 1997).

In this Letter, we investigate the effect of GR constraints on MSP spectral cutoffs, pulse profiles, integral flux, and conversion efficiency of spin-down power to γ-ray luminosity by simulating (using a finite element approach) radiative and transport processes that occur in a pulsar magnetosphere.

2. THE UNSCREENED ELECTRIC FIELD AND RADIATIVE LOSSES

We use the GR-corrected expressions for a static dipolar magnetic field (e.g., Muslimov & Tsygan 1992, hereafter MT92; MH97) and curvature radius ρ_c (e.g., HM98) of an oblique pulsar with magnetic moment $\mu = B_0 R^3/2$ inclined at an angle χ relative to the spin axis. The value of the surface magnetic field (at the pole), B_0, was solved for using (MH97)

$$\dot{E}_{\rm rot} \equiv I\Omega\dot{\Omega} \approx \frac{B_0^2\Omega^4R^6}{6c^3f^2(1)}, \tag{1}$$

with $\dot{E}_{\rm rot}$ the spin-down power, Ω the angular speed, $\dot{\Omega}$ the time derivative thereof, I the moment of inertia, R the stellar radius, c the speed of light in vacuum, and $f(\eta)$ defined by equation (25) of MT92.

The effect of GR frame dragging on the charge density, electric potential, and hence the magnitude of $E_\parallel$ (the electric field component parallel to the local magnetic field lines) was carefully modeled for the unscreened case, since the optical depth for magnetic pair production above the PC is insignificantly small (see § 3). The "near" and "far" cases for $E_\parallel$ (when $\eta \simeq 1$ and $\eta \gg 1$, with $\eta = r/R$) coincide at different points for different pulsar parameters. We use the same framework as Harding, Muslimov, and Tsygan (MT92; MH97; HM98), with all the symbols corresponding to their formalism. For the near case,

$$E_\parallel^{\rm near} = -\frac{\Phi_0}{R}\left[12\kappa\Theta_0^2 s_1\cos\chi + 6s_2\Theta_0^3 H(1)\delta(1)\sin\chi\cos\phi\right], \tag{2}$$

with the vacuum potential $\Phi_0 \equiv B_0\Omega R^2/c$, compactness param-

eter $\kappa = \epsilon I/MR^2$, $\epsilon = 2GM/Rc^2$, pulsar mass M, polar angle of the last closed magnetic field line $\Theta(\eta) = [(\Omega R\eta/cf(\eta)]^{1/2}$, and $\Theta_0 \equiv \Theta(1)$ (HM98). Furthermore, in equation (2),

$$s_1 = \sum_{i=1}^{\infty} \frac{J_0(k_i\xi)}{k_i^3 J_1(k_i)}(1 - e^{-\gamma_i(1)(\eta-1)}), \quad (3)$$

$$s_2 = \sum_{i=1}^{\infty} \frac{J_1(\tilde{k}_i\xi)}{\tilde{k}_i^3 J_2(\tilde{k}_i)}(1 - e^{-\tilde{\gamma}_i(1)(\eta-1)}), \quad (4)$$

with k_i and $\tilde{k}_i$ the positive roots of the Bessel functions J_0 and J_1, $\xi \equiv \theta/\Theta(\eta)$ the normalized polar angle, ϕ the magnetic azimuthal angle, and $H(1)\delta(1) \approx 1$. (For γ_i and $\tilde{\gamma}_i$, see eq. [22] in HM98 and definitions following eq. [43] in MT92.) Note that $E_\parallel^{\rm near}(\eta = 1) = 0$ as required by the boundary conditions and that $E_\parallel$ scales linearly with radial distance η close to the stellar surface (derived from a Taylor expansion of eqs. [3] and [4] at $\eta \sim 1$). For the far case ($\eta > R_{\rm PC}/R$), we use (HM98)

$$E_\parallel^{\rm far} \simeq -\frac{\Phi_0}{R}(1 - \xi^2)\Theta_0^2 \times \left[\frac{3}{2}\frac{\kappa}{\eta^4}\cos\chi + \frac{3}{8}\Theta(\eta)H(\eta)\delta(\eta)\xi\sin\chi\cos\phi\right], \quad (5)$$

and for the corotating charge density ρ_e, we use equation (32) in MT92.

The change in the energy of a primary electron is given (when only the dominating curvature radiation [CR] component is considered, neglecting inverse Compton [IC] scattering and synchrotron radiation) by

$$\frac{dE}{dt} = e\beta_r c E_\parallel - \frac{2}{3}\left(\frac{e^2 c}{\rho_c^2}\right)\gamma^4, \quad (6)$$

with e the electron charge, $\beta_r = v_e/c \sim 1$ the normalized electron speed, and γ the Lorentz factor. The photon energy ϵ_γ is set equal to the characteristic CR energy $\epsilon_c \equiv 1.5(\lambda_c/\rho_c)\gamma^3$ (in units of $m_e c^2$; Luo et al. 2000), with $\lambda_c = \hbar/m_e c \approx 3.86 \times 10^{-11}$ cm the Compton wavelength.

3. PAIR PRODUCTION, SPECTRA, AND CUTOFFS

According to HMZ02, the CR death line is at $\dot{E}_{\rm rot} \lesssim 10^{35}$ ergs s^{-1}. Evaluating $\dot{E}_{\rm rot} = -4\pi I\dot{P}/P^3 \sim 4 \times 10^{33}$ ergs s^{-1} (using the corrected intrinsic period derivative $\dot{P}$; Van Straten et al. 2001) suggests that no pair production will take place. Detailed modeling yields negligible optical depths, confirming this scenario. This is indeed fortunate because of the limited number of free parameters in this case. However, a low intensity of IC-scattered UV photons/soft X-rays into the TeV range may contribute to a weak pair production component.

For the parameter ranges $R_6 \equiv R/10^6$ cm = 1.3–1.7 (e.g., Kargaltsev et al. 2004), $I_{45} \equiv I/10^{45}$ g cm^2 = 1–3 (e.g., HMZ02), and $(\chi, \zeta) = (35°, 40°)$ (Manchester & Johnston 1995), $(\chi, \zeta) = (20°, 25°)$ (e.g., Pavlov & Zavlin 1997), and $(\chi, \zeta) = (20°, 16°)$ (Gil & Krawczyk 1997), with ζ the observer angle, the maximum CR cutoff energy is obtained by using $R_6 = 1.3$, $I_{45} = 3$, and $\chi = 20°$. We used $M = 1.58\ M_\odot$ derived from Shapiro delays (Van Straten et al. 2001). This corresponds to $\kappa \sim 0.2$ and surface magnetic field strength $B_8 \equiv B_0/10^8$ G ~ 7.2 (see eq. [1]). The relative altitude for maximum CR energy is obtained as $\eta \sim 1.47$, corresponding to a normalized field line colatitude of $\xi \sim 0.1$ and $\rho_c \sim 10^8$ cm, while the magnetic azimuth $\phi = 0$ results in a maximum GR potential. The analytical expression for the maximum γ-ray energy is obtained by combining equations (5) and (6) and the expression for ϵ_γ, giving

$$\epsilon_{\gamma,\,\rm max} = \left(\frac{3}{2}\right)^{7/4}\lambda_c\left(\frac{\beta_r E_\parallel}{e}\right)_{\rm max}^{3/4}\rho_c^{1/2} \lesssim 17\ \text{GeV}. \quad (7)$$

One of the most interesting predictions from MH97 is that the primary electron luminosity is given by (assuming $\chi \sim 0$)

$$L_{\rm prim,\,max}^{|\chi=0} \sim \frac{3}{4}\kappa(1 - \kappa)\dot{E}_{\rm rot}. \quad (8)$$

It is important to note that the electric potential and charge density were derived assuming that electrons leave the PC with a speed equal to c. Even if the stellar injection speed $\beta_R c \ll c$, it can be shown that the electrons will become relativistic very close to the neutron star surface, making maximum electron energies virtually independent of the injection speed (also A. K. Harding 2004, private communication). The bolometric particle luminosity of a single PC will therefore be given by (MH97)

$$L_{\rm prim} = \alpha c \int |\rho_e|\Phi\, dS, \quad (9)$$

with Φ the electric potential and dS the element of spherical surface cut by the last open field lines at radial distance r. Integrating over ξ and ϕ, and letting $\eta \to \infty$, we obtain (C. Venter 2004, unpublished)

$$L_{\rm prim,\,max} = L_{\rm prim,\,max}^{|\chi=0}\left(\cos^2\chi + \left\{\frac{3\Theta_0 H(1)[\pi/2 - \Theta_0 H(1)]}{16\kappa(1-\kappa)}\right\}\sin^2\chi\right), \quad (10)$$

providing we adopt a value of $\Theta(\eta) = \pi/2$ for distances $\eta > c/\Omega R$. This result reduces back to equation (8) when χ is set equal to zero. We calculated the maximum efficiency of conversion of pulsar spin-down power into particle luminosity $L_{\rm prim,\,max}$ for $\chi = 20°$ and $\chi = 35°$ and obtained ~2%–11% for PSR J0437−4715, for each PC (depending on R and I, using $M = 1.58\ M_\odot$). We also obtained the bolometric photon luminosity L_γ using a finite element (particle tracing) approach and integrating numerically over all photon energies and field lines from the surface to the light cylinder:

$$L_\gamma = \int_0^{\Theta_0}\int_0^{2\pi}\left[\dot{N}(\phi_R, \theta_R)\int_{r=R}^{r=c/\Omega} P_\gamma(\phi, \theta, r)dt\right]d\phi\, d\theta. \quad (11)$$

Here P_γ is the CR photon power integrated over frequency and $\dot{N} = \rho_e c\, dS/e$ the number of particles ejected per second from a PC surface patch dS at $r = R$ centered at (ϕ_R, θ_R). Since we cannot start with $\beta_R = 1$ (i.e., infinite Lorentz factor), we assumed values close to 1 and found convergent photon luminosities of 2%–9% of the spin-down power (depending on R,

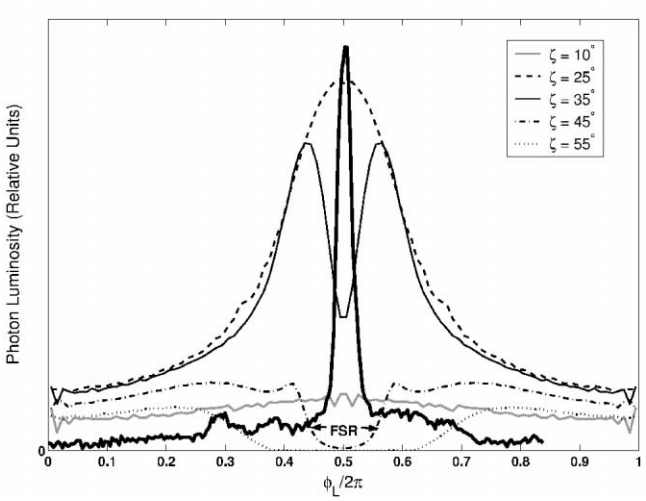

FIG. 1.—Photon luminosity (in relative units) vs. observer pulse phase (with phase 0.5 corresponding to either $\phi = 0$ or $\phi = \pi$, depending on ζ) for PSR J0437−4715 for different ζ (see legend). The following parameters were assumed (see text for references): $P \approx 5.76$ ms (period), $R_6 = 1.3$, $I_{45} = 1$, $M = 1.58\ M_\odot$, and $\chi = 35°$. The radio pulse at 4.6 GHz (*thick solid line*; Manchester & Johnston 1995) is superimposed for reference (see http://www.atnf.csiro.au/research/pulsar/psrcat). The "valleys" at observer phase ~0.5 of the light curves with $\zeta \geq \chi$ are probably due to electric field sign reversals (FSR), since the magnetic field lines where these reversals occur were ignored (see text for details).

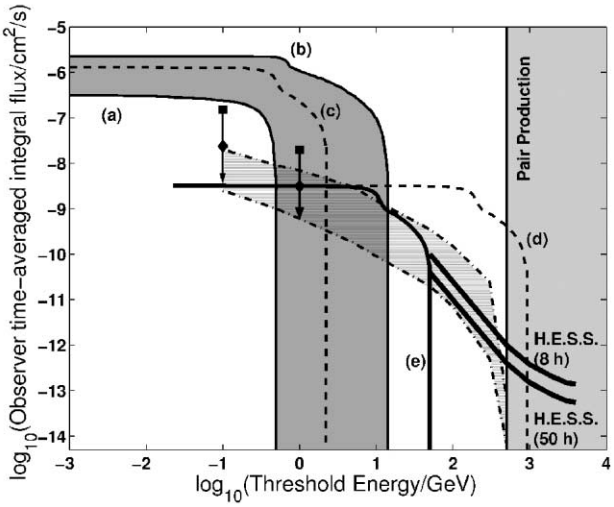

FIG. 2.—Observer time-averaged integral flux vs. threshold energy. Curve *a*, for which $R_6 = 1.7$, $I_{45} = 1$, $\chi = 35°$, and $\zeta = 40°$, and curve *b*, for which $R_6 = 1.3$, $I_{45} = 3$, $\chi = 20°$, and $\zeta = 16°$, define a "confidence band" wherein the integral flux is expected to lie according to the GR model discussed in this Letter. Curve *c*, for which $R_6 = 1.5$, $I_{45} = 2$, $\chi = 20°$, and $\zeta = 16°$, represents an intermediate curve. Curve *d* is curve *c* scaled with scale factor $\lambda = 400$, while curve *e* is curve *d* shifted to the left (see text for details). The band with dot-dashed curves is that of BRD00 for PSR J0437−4715 for their model A. The squares represent EGRET integral flux upper limits (Fierro et al. 1995), while the diamonds represent these upper limits reduced by a factor of $\sqrt{5}$, appropriate for a beam with a main pulse width of ~0.2. Also indicated are the H.E.S.S. sensitivities for 50 hr (Hinton 2004) and 8 hr observation time and the energy above which pair production is expected to take place (BRD00).

I, χ, and ζ), i.e., $L_\gamma/L_{\rm prim,\,max} \sim 1$. This means that almost all particle luminosity is converted to photon luminosity as expected for strong radiation reaction. Radiation reaction, combined with further (weak) acceleration toward the light cylinder, results in a total residual electron power of ~1%–2.5% of the spin-down power at the light cylinder.

It should be noted that the fundamental unscreened expression for $E_\parallel$ (eq. [5]) changes sign along ~40% of the magnetic field lines originating at the PC. This field reversal is most dominant when $\phi \sim \pi$, whereas no field reversals occur for $\phi \sim 0$. Trapping of electrons may ensue at magnetic field lines along which the electric field reverses. We expect the system to reach a steady state as a result of the redistribution of charges along these field lines. These lines may become equipotential lines, or a reduced current may develop, resulting in the suppression of particle acceleration along them. This justifies our neglect of these field lines when calculating the pulse profiles, bolometric photon luminosity, and integral flux.

Figure 1 shows the pulse profiles for different observer angles ζ, for $\chi = 35°$. Maximum observed photon flux is obtained for $\zeta \sim \chi$ and for large values of $\cos\phi$ (as in eq. [5]). The "dip" in light curves with $\zeta \geq \chi$ near phase $\phi_L/2\pi \sim 0.5$ (where $\phi \sim \pi$) might be due to the sign reversal of the electric field, because the magnetic field lines where this sign reversal occurs were ignored, as noted above.

The differential photon power $dL_\gamma(\phi_L,\ \zeta,\ E)/d\phi_L\, d\zeta\, dE$ per phase bin $d\phi_L$, per observer angle bin $d\zeta$, per energy bin dE, is obtained by inserting the product of the ratios of indicator functions $I(\phi_L,\ \phi_L + d\phi_L)$, $I(\zeta,\ \zeta + d\zeta)$, and $I(E,\ E + dE)$ and their respective bin widths $d\phi_L$, $d\zeta$, and dE in the integrand of equation (11). This allows us to compare the expected integral photon flux with EGRET upper limits above 100 MeV and 1 GeV (Fierro et al. 1995) as well as with forthcoming High Energy Stereoscopic System (H.E.S.S.) observations of this pulsar (C. Venter 2004, unpublished). Note that the imaging threshold energy of H.E.S.S. is ~100 GeV (Hofmann 2001), although a nonimaging "pulsar trigger" for timing studies down to $\gtrsim$50 GeV can be employed for pulsar studies with H.E.S.S. (de Jager et al. 2001).

The phase-averaged photon flux (as would be seen on a DC sky map) for a single PC may be calculated by

$$\bar{F}^o_\gamma(>E) = \frac{\beta^o}{d^2\Delta\Omega^o}\int_E^\infty \int_\zeta^{\zeta+d\zeta}\int_0^{2\pi} \frac{1}{E'}\left[\frac{dL(\phi'_L,\ \zeta',\ E')}{d\phi'_L\, d\zeta'\, dE'}\right] d\phi'_L\, d\zeta'\, dE', \tag{12}$$

with distance $d = 139$ pc, $\beta^o = \Delta\phi_L/2\pi$, $\Delta\phi_L$ the pulse width in units of radians, $\Delta\Omega^o(>E) = \sin\zeta\, d\zeta\Delta\phi_L$ the beaming solid angle, and $d\zeta$ taken arbitrarily small. Only one PC is expected to be seen, given the relative orientations of the magnetic axis and observer line of sight to the spin axis. The superscript "o" is used to indicate quantities applicable to an observer with $\zeta \in (\zeta,\ \zeta + d\zeta)$.

The energy spectrum dL/dE due to CR is quite hard, resulting in a constant time-averaged integrated photon flux $F^o_\gamma(>E)$, seen by the observer, as shown in Figure 2 (e.g., curves *a* and *b*). The 100 MeV and 1 GeV EGRET flux upper limits from Fierro et al. (1995) are indicated by the squares in Figure 2, which clearly constrain the flux band defined by curves *a* and *b*. If we define an a priori phase interval of $\beta^o \sim 0.2$, centered on the radio pulse, and recalculate the EGRET flux upper limits from the factor of 5 ($=1/\beta^o$) reduced sky map background, we should get the even more constraining upper limits given by the diamonds in Figure 2. We therefore have to revise the predicted fluxes for PSR J0437−4715, and we do so based on

the following scaling argument: If we assume that the particle and hence γ-ray luminosity only scales with the spin-down power and neutron star compactness, as in equations (8) and (10), i.e., the product of the current and voltage for such a pair-starved pulsar is a constant as predicted by equation (8), we may scale the set of curves *a*–*c* (according to this condition of a constant photon luminosity L^o_γ) in terms of the limiting voltage and hence the cutoff energy to give $F^o_{\gamma,1}(>E_1)E_{\rm cutoff,1} \sim F^o_{\gamma,2}(>E_2)E_{\rm cutoff,2}$ (for constant β^o and $\Delta\Omega^o$, and energies $E_1 < E_2$; $E_{\rm cutoff,1} < E_{\rm cutoff,2}$). In particular, when curve *c* is scaled according to $E_{\rm cutoff,2} = \lambda E_{\rm cutoff,1}$, implying $F^o_{\gamma,2}(>E_2) \sim F^o_{\gamma,1}(>E_1)/\lambda$, with $\lambda = 400$, curve *d* is obtained, which no longer violates the revised EGRET upper limit at 1 GeV, but the cutoff energy then shifts up to ~1 TeV. Furthermore, if curve *d* is now translated so that the energy cutoff also falls below the H.E.S.S. sensitivity curves, curve *e* is obtained, which would be consistent with both EGRET and H.E.S.S. (if the latter instrument does not detect this pulsar). Also shown is the flux band calculated for PSR J0437−4715 by BRD00. Again, for a power-law photon spectrum with exponential cutoff, it can be shown that $F^o_\gamma(>E_1)E_{\rm cutoff} \sim \beta^o L^o_\gamma/d^2\Delta\Omega^o$ [assuming $E_1 \ll E_{\rm cutoff}$ and $F^o_\gamma(>E)$ has a flat slope due to CR]. In order to constrain PSR J0437−4715's bolometric photon luminosity by forthcoming H.E.S.S. observations, we postulate that $L_\gamma = \alpha L^o_\gamma$, where $\alpha = \alpha(\chi, \zeta) \gg 1$ is a geometrical factor correcting from the incremental luminosity corresponding to the observer's line of sight to the total γ-ray luminosity of the pulsar. It then follows that $L_\gamma \sim xF^o_\gamma(>E_1)E_{\rm cutoff}$, with $x(\chi, \zeta) = \alpha d^2 2\pi \sin\zeta\, d\zeta$, which was found to be more or less constant for the same χ and ζ. A nondetection by H.E.S.S., as implied by curve *e*, leads to a γ-ray luminosity of $\lesssim 0.003\dot{E}_{\rm rot}$. This value should be compared with the prediction of $L_\gamma \sim 3 \times 10^{-5}\dot{E}_{\rm rot}$ given by Rudak & Dyks (1999) for a canonical pulsar with $P = 1$ ms and $B_0 = 10^9$ G and with $L_\gamma \sim 0.04\dot{E}_{\rm rot}$ predicted for pair-starved pulsars with off-beam geometry (using $P \approx 5.76$ ms and $\dot{E}_{\rm rot} \sim 4 \times 10^{33}$ ergs s^{-1}; Muslimov & Harding 2004).

4. CONCLUSIONS

CR cutoff energies for MSPs such as PSR J0437−4715 were predicted to be in the range 50–100 GeV by HMZ02 and BRD00, making proposals for ground-based telescopes with imaging thresholds near 100 GeV (e.g., H.E.S.S. [Hofmann 2001] and CANGAROO [Yoshida et al. 2002]) attractive. From the present GR theory, one would conclude that these telescopes may not be able to see the spectral tail corresponding to the intense primary CR component, since the hard primary CR spectrum does not extend to energies above ~20 GeV, as verified by both analytical and numerical (finite element) approaches. An IC component resulting from TeV electrons scattering the UV/soft X-rays from the surface of PSR J0437−4715 may, however, still be detectable, although this prediction by BRD00 should also be reevaluated within a GR electrodynamic framework. However, it is quite obvious that the predicted time-averaged observer flux violates the EGRET upper limit at 100 MeV, implying a revision of the existing theory. Forthcoming H.E.S.S. and future *Gamma-Ray Large Area Space Telescope* observations will help to constrain the γ-ray luminosity and therefore the accelerating electric field.

The authors would like to acknowledge useful discussions with A. K. Harding, B. Rudak, and A. Konopelko. This publication is based on work supported by the South African National Research Foundation under grant 2053475.

REFERENCES

Bulik, T., Rudak, B., & Dyks, J. 2000, MNRAS, 317, 97 (BRD00)
de Jager, O. C., Konopelko, A., Raubenheimer, B. C., & Visser, B. 2001, in AIP Proc. 558, High Energy Gamma-Ray Astronomy, ed. F. A. Aharonian & H. J. Völk (Melville: AIP), 613
Dyks, J., Rudak, B., & Bulik, T. 2001, in Exploring the Gamma-Ray Universe, ed. B. Battrick (ESA SP-459; Noordwijk: ESA), 191
Fierro, J. M., et al. 1995, ApJ, 447, 807
Gil, J., & Krawczyk, A. 1997, MNRAS, 285, 561
Harding, A. K., & Muslimov, A. G. 1998, ApJ, 508, 328 (HM98)
Harding, A. K., Muslimov, A. G., & Zhang, B. 2002, ApJ, 576, 366 (HMZ02)
Hinton, J. A. 2004, NewA Rev., 48, 331
Hofmann, W. 2001, Proc. 27th Int. Cosmic-Ray Conf. (Hamburg), OG2.5, 2785
Johnston, S., et al. 1993, Nature, 361, 613
Kargaltsev, O., Pavlov, G. G., & Romani, R. W. 2004, ApJ, 602, 327
Luo, Q., Shibata, S., & Melrose, D. B. 2000, MNRAS, 318, 943
Manchester, R. N., & Johnston, S. 1995, ApJ, 441, L65
Muslimov, A. G., & Harding, A. K. 1997, ApJ, 485, 735 (MH97)
———. 2003, ApJ, 588, 430
———. 2004, ApJ, 617, 471
Muslimov, A. G., & Tsygan, A. I. 1992, MNRAS, 255, 61 (MT92)
Pavlov, G. G., & Zavlin, V. E. 1997, ApJ, 490, L91
Rudak, B., & Dyks, J. 1999, MNRAS, 303, 477
Usov, V. V. 1983, Nature, 305, 409
Van Straten, W., Bailes, M., Britton, M. C., Kulkarni, S. R., Anderson, S. B., Manchester, R. N., & Sarkissian, J. 2001, Nature, 412, 158
Yoshida, T., Yoshikoshi, T., & Yuki, A. 2002, Astropart. Phys., 16, 235
Zavlin, V. E., Pavlov, G. G., Sanwal, D., Manchester, R. N., Trümper, J., Halpern, J. P., & Becker, W. 2002, ApJ, 569, 894